RSC Advances

PAPER

View Article Online
View Journal | View Issue

Cite this: *RSC Adv.*, 2019, **9**, 36034

Facile liquid-assisted one-step sintering synthesis of superfine $L1_0$-FePt nanoparticles

Wenli Pei, *[a] Dong Zhao, [a] Chun Wu, *[b] Xiaoyang Wang,[c] Kai Wang,[c] Jianjun Wang[a] and Qiang Wang [c]

Received 2nd September 2019
Accepted 21st October 2019

DOI: 10.1039/c9ra06966f

rsc.li/rsc-advances

A liquid-assisted one-step sintering method was proposed for the synthesis of $L1_0$-FePt superfine nanoparticles. The liquid assisted Fe and Pt precursors were homogeneously deposited on NaCl media, which facilitated the nucleation rates, obviously reduced the particle size and promoted the orderly transformation. Through optimizing the sintering parameters, superfine $L1_0$-FePt nanoparticles (about 7 nm, TEM) with coercivity as high as 2.29 T were obtained. This research highlights the feasibility of synthesizing $L1_0$-FePt nanoparticles with superfine sizes and ultra-high coercivity.

Introduction

FePt nanoparticles (NPs) with fct ($L1_0$) structures have received considerable attention for their potential applications in permanent magnets, high-density magnetic recording media, and high-efficiency catalysts.[1–3] These application performances are closely related to the morphology, size, and crystal structures of the particles. The FePt NPs with small size, uniform morphology and high structural ordering are in high demand. Since the initial report by Sun *et al.*,[4] chemical synthesis has become an extensive route for the fabrication of FePt NPs.[5–9] Normally, the FePt NPs directly synthesized by chemical methods are of the fcc structure. In order to obtain good performance, the particles should be transformed from the fcc to the fct structure by post-annealing. However, the particles would grow and aggregate during this treatment, which seriously worsens the performance of the NPs and limits their application; many efforts have been made toward solving this bottleneck problem. Some materials such as SiO_2, MgO, and NaCl have been employed as the protective inert layer or matrix to restrict grain growth and aggregation;[10–12] however, the effects have been limited and abnormally large particles and aggregation were still not avoided.

Some previous works have shown that the direct synthesis of $L1_0$-FePt nanomaterials in high-boiling-temperature solvents results in limited structural ordering.[13,14] To achieve a higher-ordered structure, a third element doping method, with elements such as Cu, Ag, Au and Bi, has been employed to accelerate the $L1_0$ ordering or promote crystallographic orientation.[15–18] However, to date, the FePt NPs prepared by the direct wet chemical synthesis route show a partial structural ordering that is not high enough for further applications.

Recently, a simple one-step solid-phase approach to the preparation of $L1_0$-FePt NPs has been reported.[19] In this method, Fe and Pt precursors are used in the absence of an organic solvent and surfactant, NaCl particles are employed as the substrate for nanoparticle nucleation and growth, as well as an insulation medium preventing nanoparticle coalescence during high-temperature sintering. The chemically ordered $L1_0$-FePt NPs with coercivity of more than 2 T can be obtained. Although this method is a promising route, the as-prepared particles are hard to control, and it is difficult to synthesize superfine NPs. The synthesis of the superfine NPs with high degree of order is anticipated for the application of $L1_0$-FePt NPs.

In this work, we report a modified one-step sintering method in which a liquid-assistant process is employed. The precursors were dissolved in the solvent and then the solution was mixed with fine NaCl powder. The mixture was heated under strong stirring until the liquid evaporated; thus, the precursors could uniformly precipitate on the surface of the NaCl particles. The solid mixture was then sintered to obtain $L1_0$-FePt NPs directly. The relationships among synthesis process, particle size, and ordering degree are discussed herein, and the optimal process for preparing FePt NPs with a superfine size and good performance is studied. This liquid-assisted method offers a good solution to the uniformity problem of solid–solid mixing in previous reports and is a promising facile method for synthesizing superfine $L1_0$-FePt NPs.

Experimental methods

$Pt(acac)_2$ and $Fe(acac)_3$ were employed as precursors. Hexane was used as a liquid solvent to dissolve the precursors. NaCl as

[a]Key Laboratory of Anisotropy and Texture of Materials (Ministry of Education), Northeastern University, Shenyang 110819, People's Republic of China. E-mail: peiwl@atm.neu.edu.cn

[b]School of Materials Science and Engineering, Liaoning Technical University, Fuxin 123000, People's Republic of China. E-mail: chun_wu@126.com

[c]Key Laboratory of Electromagnetic Processing of Materials (Ministry of Education), Northeastern University, Shenyang 110819, People's Republic of China

an insulator was milled into a micro-scale powder with particle size smaller than 10 μm. These reagents were obtained from commercial sources and used without further purification.

For preparing $L1_0$-FePt NPs, the metal precursors $Fe(acac)_3$ (0.25 mmol, about 0.088 g) and $Pt(acac)_2$ (0.25 mmol, about 0.100 g) were dissolved in 50 mL of hexane, and then sodium chloride (NaCl 75 g, the mass ratio of precursors to insulator was set as 1/400) was added to the solution. The mixture was heated to 80 °C under strong stirring. After evaporation of the solvent, the mixture was moved to a quartz boat. The quartz boat was heated in a tube furnace at the rate of 10 °C min^{-1} under a reducing atmosphere (5%H_2 + Ar). For the controllable synthesis of $L1_0$-FePt NPs, the sintering temperature was tuned from 300 to 750 °C and the mass ratio of the precursors to insulator was increased from 1/400 to 1/100. The $L1_0$-FePt NPs were collected by centrifugal washing, repeatedly with water and alcohol, and stored in alcohol at −20 °C.

The NPs specimens for transmission electron microscopy (TEM, JEM-2100F, 200 kV) analysis were prepared by drying a dispersion of the NPs on amorphous carbon-coated copper grids. Grain sizes of the NPs were determined by counting more than 100 particles in the TEM images by using Win Roof software. The crystal structure and lattice parameters of the NPs were measured by a standard powder X-ray diffraction method (XRD, Ultima IV, Cu K_α). Magnetic properties of the NPs were characterized through the superconducting quantum interference device (Quantum Design, MPMS3).

Results and discussion

The XRD patterns of the FePt NPs sintered from 300 to 750 °C are shown in Fig. 1. At 300 °C and 500 °C, the FePt NPs were in the disordered fcc-phase, and the diffraction peaks from the (111), (200) and (220) faces could be detected. Some diffraction peaks from NaCl were also found when the sintering temperature was lower. Above 600 °C, all the diffraction peaks can be indexed as the $L1_0$-phase with the fct structure (CIF. 1540807), which means the orderly fcc–fct transformation occurred at 600 °C in the liquid-assisted sintering process. The transformation temperature in this work is higher than that in previous reports without liquid-assistance (350 °C).[19] The diffraction peaks of (200) and (002) become more obvious when increasing the sintering temperature, indicating an increase in the order degree of the NPs.

The JADE software was used to calculate the lattice parameters. The lattice parameter a of the fcc-FePt phase was calculated from the diffraction angles of the (111) and (200) peaks. The lattice parameter c of the fct-FePt phase was calculated from the diffraction angles of the (001) and (002) peaks, and another lattice parameter a was calculated from the diffraction angles of the (110) and (200) peaks. The calculated lattice parameter values are shown in Fig. 2(a). The a of fcc-FePt is between that of fcc-Fe (PDF. 89-4185, 0.3649 nm) and fcc-Pt (PDF. 88-2343, 0.3970 nm), it decreases on increasing the sintering temperature from 300 °C to 500 °C, which means a composition evolution is induced and the Fe content in fcc-FePt NPs is increased to generate a Fe-rich fcc-phase.[20] These results also agree with the composition evolution of FePt NPs, as shown in Fig. 2(c). Both a and c of fct-FePt decreased and became, close to the standard values (a_{sf} = 0.3849 nm, c_{sf} = 0.3700 nm, CIF. 1540807) on further increasing the sintering temperature from 650 °C to 750 °C. The order degree s was calculated by the formula $s^2 = [1 - (c/a)]/[1 - (c/a)_{sf}]$. As shown in Fig. 2(b), s increased with the sintering temperature. The results prove that the order degree of the $L1_0$-FePt phase can be enhanced by increasing the temperature because higher temperatures benefit the orderly transformation. Fig. 2(c) shows the composition evolution of sintered FePt NPs; less Fe alloys with Pt when sintered with liquid-assistance at 300 °C and 500 °C. The Fe and Pt contents in the FePt NPs are close when the temperature increases to above 600 °C. Considering that the fct-FePt phase is also generated at above 600 °C, it can be deduced that the composition also has a significant influence on the orderly transformation, besides the sintering temperature.

TEM images of the $L1_0$-FePt NPs sintered from 600 °C to 750 °C are shown in Fig. 3(a)–(d). At various sintering temperatures, almost all the $L1_0$-FePt particles are sphere-like and

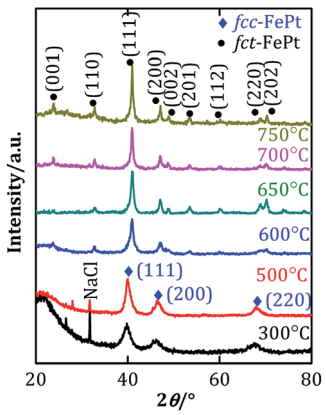

Fig. 1 XRD patterns of FePt NPs sintered at various temperatures.

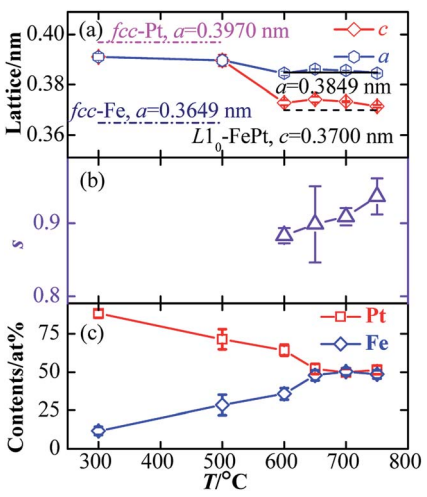

Fig. 2 Lattice parameters (a), order degree (b), and composition (c) of FePt NPs sintered at various temperatures.

monodisperse; the aggregation of a few of the NPs might be related to the magnetic interaction and surfactant-free surfaces.[19,21] Fig. 3(e) shows the SAED image of the $L1_0$-FePt particles sintered at 600 °C; the diffraction rings are indexed as the faces of the $L1_0$-FePt phases and they agreed well with the XRD results. The as-prepared NPs were single crystals, as confirmed by the HRTEM images from Fig. 3(f). The uniform fringes were distributed throughout the particles and the interplanar spacing was indexed as the (110) face of the $L1_0$-FePt.

The grain size distributions of the $L1_0$-FePt NPs sintered at different temperatures are shown in Fig. 4(a). The distributions were well fitted with the Gauss function, which indicates that the growth model of the $L1_0$-FePt NPs is a typical ripening process[22] because the NaCl insulator restricts the attachment of the surfactant-free magnetic NPs. The mean grain sizes of the $L1_0$-FePt NPs calculated from the Scherrer formula (XRD patterns) and Gauss functions (TEM images) are shown in Fig. 4(b) and listed in Table 1. The errors in grain sizes (TEM) originated from the standard deviation of the Gaussian function. The sizes determined by the Scherrer formula are larger as compared to the Gauss function, which might be caused by the aggregation while preparing the samples for XRD. Nevertheless, the grain sizes of the $L1_0$-FePt NPs calculated by both methods presented similar trends, and the sizes increased with the increasing sintering temperature because the temperature accelerated the element diffusion in ripening growth.[22] It should be noted that the $L1_0$-FePt nanoparticles obtained from the liquid-assisted method were smaller than the NPs prepared in the absence of liquid, which might be attributed to the modification of the growth process. The uniform distribution of precursors on the NaCl insulator enhanced the nucleation rate and regulated the growth rate of the $L1_0$-FePt nanoparticles. The quantity of nanoparticles with a size smaller than 3 nm, which are over-fine and present a superparamagnetic performance, is reduced as the sintering temperature increases (Fig. 4(c)). The

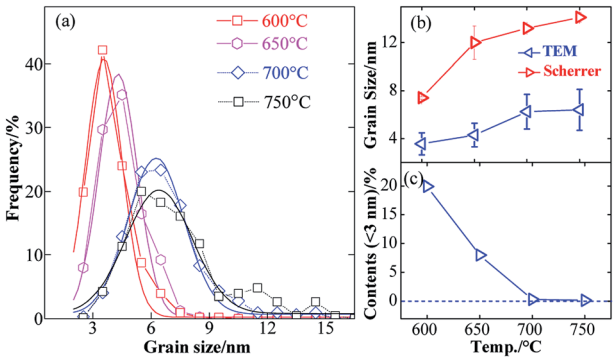

Fig. 4 Grain size distributions (a), grain sizes (b), and over-fine NPs contents (c) of the $L1_0$-FePt NPs synthesized at various temperatures.

number of over-fine particles decreases to nearly zero when the sintering temperature increases to above 700 °C. In addition, the quantity of abnormally grown $L1_0$-FePt NPs (the particles with sizes twice that of the main particle size) increased with increasing sintering temperature. Although increasing the sintering temperature can reduce the superparamagnetic fcc-FePt NPs (size below 3 nm) and guarantee the consistency of the phases in the products, it will increase the size range and destroy the size uniformity. Therefore, more sintering parameters need to be optimized to ensure the size uniformity of the $L1_0$-FePt NPs.

The room temperature magnetic hysteresis loops of the $L1_0$-FePt NPs are shown in Fig. 5(a). The coercivity (Fig. 5(b)) of the $L1_0$-FePt NPs obtained at 600 °C, 650 °C, 700 °C and 750 °C are 0.20, 0.55, 1.02, and 2.17 T, respectively. The increased degree of order, s, and grain size led to the enhancement of the coercive field, which was comparable to previous reports. The $L1_0$-FePtBi nanoparticles of size 21 nm, with $s = 0.91$, showed a coercive field of 1.52 T.[18] An obvious kink was observed in the magnetic hysteresis loops of the $L1_0$-FePt NPs sintered at 600 °C and

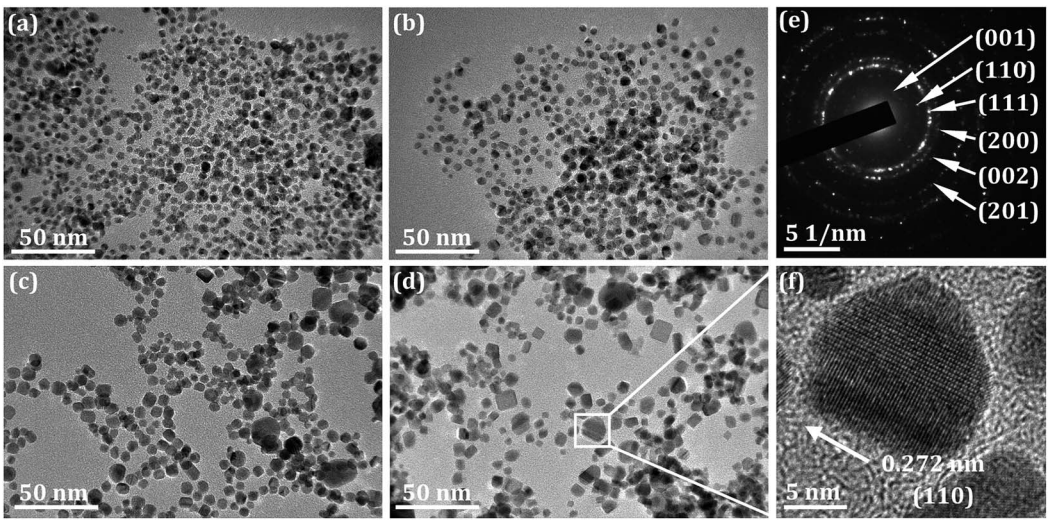

Fig. 3 TEM images of $L1_0$-FePt NPs sintered at various temperatures. (a) 600 °C, (b) 650 °C, (c) 700 °C, (d) 750 °C. (e) SAED image of $L1_0$-FePt nanoparticle sintered at 600 °C. (f) HRTEM image of $L1_0$-FePt nanoparticle.

Table 1 Sintering conditions, grain sizes, order degree *s*, coercivity, and remanence ratio of $L1_0$-FePt NPs

T/°C	$m_{(Fe+Pt)}/m_{NaCl}$	Size/nm (TEM)	d/nm (XRD)	s	H_c/T	M_r/M_s
600	1/400	3.56 ± 0.93	7.4 ± 0.1	0.883	0.20	0.35
650		4.29 ± 0.99	12.0 ± 1.4	0.898	0.55	0.43
700		6.25 ± 1.45	13.2 ± 0.3	0.909	1.02	0.53
750		6.40 ± 1.70	14.1 ± 0.4	0.936	2.17	0.58
700	1/100	7.30 ± 2.16	28.0 ± 1.2	0.940	2.29	0.61

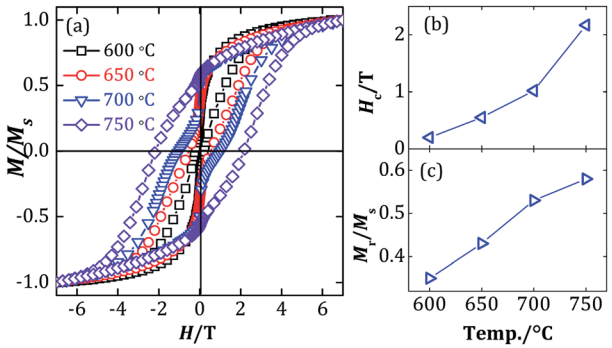

Fig. 5 Magnetic hysteresis loops (a), coercivity (b), and remanence ratio (c) of the $L1_0$-FePt NPs synthesized at different temperatures.

650 °C, due to the existence of the superparamagnetic FePt NPs.[19,21,23] On increasing the sintering temperature, the quantity of superparamagnetic FePt NPs decreased. Therefore, the kink in the magnetic hysteresis loops was lower at 700 °C and 750 °C, and the rectangular ratios increased. By introducing the liquid-assisted method, superfine $L1_0$-FePt NPs of 6.5 nm (TEM) with high coercivity (2.17 T) could be obtained at 750 °C.

For the further controllable preparation of $L1_0$-FePt NPs, the precursor concentration $m_{(Fe+Pt)}/m_{NaCl}$ increased from 1/400 to 1/100. Since the grain size distribution is wide at 750 °C, the $L1_0$-FePt NPs were sintered at 700 °C at the concentration of 1/100 to ensure size uniformity. The TEM image of the as-prepared NPs is shown in Fig. 6(a); the NPs are still sphere-like and monodisperse. The grain size distribution of the NPs is shown in Fig. 6(b), and the grain sizes of the NPs sintered at different conditions are summarized in Table 1. Increasing the sintering temperature from 700 °C to 750 °C increased the average grain size and enlarged the distribution width. However, changing the concentration from 1/400 to 1/100 only increased the grain size but showed no obvious influence on the uniformity of the size distributions. The XRD pattern of the $L1_0$-FePt NPs sintered at higher concentration is shown in Fig. 6(c), and *s* is listed in Table 1 to be even higher than that of the sample prepared at 750 °C. The magnetic hysteresis loops are shown in Fig. 6(d); there was no kink for the $L1_0$-FePt NPs sintered at higher concentration, and the coercivity was also higher than that of the sample prepared at 750 °C. Thus, it can be concluded that the precursors with a reasonable concentration are beneficial for controlling grain sizes, enhancing the order degree, and optimizing the hard magnetic properties of the sintered $L1_0$-FePt NPs.

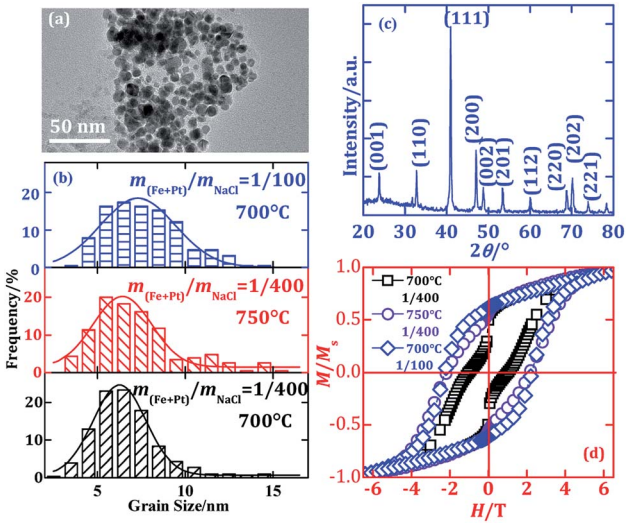

Fig. 6 TEM image (a), grain sizes distributions (b), XRD pattern (c), and magnetic hysteresis loops (d) of $L1_0$-FePt NPs synthesized by varying the concentration.

Compared with the previous report (the $L1_0$-FePt NPs sintered without liquid), the employment of the liquid-assisted method can refine the grain sizes, ensure the size uniformity, enhance the order degree, and optimize the hard-magnetic properties. The possible reason is that the process of formation of FePt NPs is different in the two reactive systems. The schematic diagrams of the two systems are shown in Fig. 7.

When sintering without liquid-assistance, the micron-sized precursor particles are mixed together. Most of the precursors are located at the intersection spaces among NaCl particles, as shown in Fig. 7(a_1). During the sintering process, the Fe and Pt precursors decomposed, then, Fe and Pt clusters were generated in these spaces, as shown in Fig. 7(a_2). Finally, the high temperature drove the alloying process of the Fe and Pt clusters, and the $L1_0$-FePt NPs were formed by consuming the adjacent Fe and Pt clusters, as seen in Fig. 7(a_3). The size and composition of the obtained particles have close relationships with the homogeneity of the mixed precursors and the spaces among NaCl particles, which are hard to control. Therefore, it is difficult to obtain superfine and homogeneous $L1_0$-FePt NPs.

With the liquid-assisted method, the Fe and Pt precursors were homogeneously mixed and uniformly deposited on NaCl particles, and a special NaCl@Precursors core–shell structure was formed, as shown in Fig. 7(b_1). Normally, the nuclei are likely to be generated in the areas with rich precursors, and the NaCl particles surrounded by the precursor shell provide a good medium for generating the nuclei. Therefore, there are more suitable nucleation sites in this method. More nuclei grew simultaneously, which led to a significant decrease in the particle size and the improvement of the uniformity of the particles. The uniform composition distribution also benefits the orderly transformation, because the diffusion of Fe and Pt elements is easy and consistent. The FePt clusters were directly generated on the NaCl mediums, as seen in Fig. 7(b_2). Finally, the $L1_0$-FePt NPs grow by consuming the smaller FePt clusters,

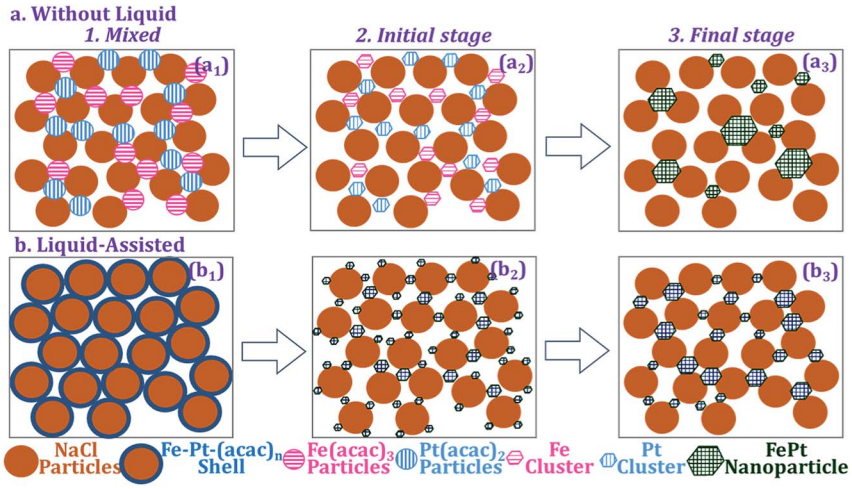

Fig. 7 Schematic diagram illustrates the formation process of $L1_0$-FePt NPs in the presence or absence of liquid-assisted. (a) Without liquid method, and (b) liquid-assisted method.

as shown in Fig. 7(b_3). The Fe content in the FePt NPs is lower than that of Pt at lower reactive temperatures, such as 300 °C and 500 °C, because the Fe precursor is more difficult to reduce. When the sintering temperature is high enough for decomposing lower concentrations of $Fe(acac)_3$, such as above 600 °C, the atomic ratio of Fe and Pt is close to 1 : 1, and this reasonable composition drives the fcc–fct transformation to occur simultaneously. Therefore, this liquid-assisted method is favorable for preparing the ordered structure and obtaining superfine particles.

Conclusions

The $L1_0$-FePt nanoparticles with superfine size (about 7 nm, TEM) and high coercivity (up to 2.29 T) were successfully synthesized by the liquid-assisted sintering method. With the assistance of liquid, the precursors formed a shell with uniform composition and size on a NaCl medium, which increased the nucleation rate, promoted the orderly transformation, and thus improved the hard-magnetic properties. In this process, the Fe and Pt atoms increased to equal ratio, and the fcc–fct transformation occurred at 600 °C. Increasing the temperature increased the grain size, widened the size distribution, enhanced the order degree and improved the hard-magnetic properties of $L1_0$-FePt nanoparticles. Reasonably increasing the precursor concentration could also increase the grain size, enhance the order degree, and improve the hard-magnetic properties; in particular, it guaranteed the size uniformity. These results indicate that liquid-assistance is a feasible strategy for synthesizing $L1_0$-FePt nanoparticles with superfine size and ultra-high coercivity.

Conflicts of interest

There are no conflicts to declare.

Acknowledgements

This work was financially supported by the National Natural Science Foundation of China (Grant No. 51871045, 51690161, 51425401), Liaoning Innovative Research Team in University (Grant No. LT2017011), the Fundamental Research Funds for the Central Universities (Grant No. N160907001, N180912004), and the Doctoral Scientific Research Foundation of Liaoning Province (Grant No. 2019-BS-116).

References

1 S. Sun, C. B. Murray, D. Weller, L. Folks and A. Moser, *Science*, 2000, **31**, 1989–1992.
2 H. Zeng, J. Li, J. P. Liu, Z. L. Wang and S. Sun, *Nature*, 2002, **420**, 395–398.
3 J. Wang, Z. Wang, S. Li, R. Wang and Y. Song, *Nanoscale*, 2017, **9**, 4066–4075.
4 S. Sun, *Adv. Mater.*, 2006, **37**, 393–403.
5 Z. Meng, G. Li, H. F. Wong, S. M. Ng, S. C. Yiu, C. L. Ho, C. W. Leung, I. Manners and W. Y. Wong, *Nanoscale*, 2016, **9**, 731–738.
6 B. Bian, W. Xia, J. Du, J. Zhang, J. P. Liu, Z. Guo and A. Yan, *Nanoscale*, 2013, **5**, 2454–2459.
7 C. Wu, X. Wang, W. Pei, D. Zhao, K. Wang, G. Li and Q. Wang, *Nanoscale*, 2019, **11**, 15023–15028.
8 X. Duan, C. Wu, X. Wang, X. Tian, W. Pei, K. Wang and Q. Wang, *J. Alloys Compd.*, 2019, **797**, 1372–1377.
9 C. Wu, W. Pei, X. Wang, K. Wang, G. Li and Q. Wang, *RSC Adv.*, 2016, **6**, 84684–84688.
10 Y. Tamada, S. Yamamoto, M. Takano, S. Nasu and T. Ono, *Appl. Phys. Lett.*, 2007, **90**, 162509.
11 J. Kim, C. Rong, J. P. Liu and S. Sun, *Adv. Mater.*, 2009, **21**, 906–909.
12 C. Rong, N. Poudyal, G. S. Chaubey, V. Nandwana, Y. Liu, Y. Q. Wu, M. J. Kramer, M. E. Kozlov, R. H. Baughman and J. P. Liu, *J. Appl. Phys.*, 2008, **103**, 07E131.

13 L. E. M. Howard, H. L. Nguyen, S. R. Giblin, B. K. Tanner, I. Terry, A. K. Hughes and J. S. O. Evans, *J. Am. Chem. Soc.*, 2005, **127**, 10140–10141.
14 W. Lei, Y. Yu, W. Yang, M. Feng and H. Li, *Nanoscale*, 2017, **9**, 12855–12861.
15 Y. Yu, P. Mukherjee, Y. Tian, X. Z. Li, J. E. Shield and D. J. Sellmyer, *Nanoscale*, 2014, **6**, 12050–12055.
16 H. Wang, P. Shang, J. Zhang, M. Guo, Y. Mu, Q. Li and H. Wang, *Chem. Mater.*, 2013, **25**, 2450–2454.
17 H. Wang, Y. Li, X. Chen, D. Shu, X. Liu, X. Wang, J. Zhang, H. Wang, Y. Wang and P. Ruterana, *J. Magn. Magn. Mater.*, 2017, **422**, 470–474.
18 F. M. Abel, V. Tzitzios, E. Devlin, S. Alhassan, D. J. Sellmyer and G. C. Hadjipanayi, *ACS Appl. Nano Mater.*, 2019, **2**, 3146–3153.
19 J. He, B. Bian, Q. Zheng, J. Du, W. Xia, J. Zhang, A. Yan and J. P. Liu, *Green Chem.*, 2016, **18**, 417–422.
20 C. Wu, K. Wang, D. Li, C. Lou, Y. Zhao, Y. Gao and Q. Wang, *J. Magn. Magn. Mater.*, 2016, **416**, 61–65.
21 C. N. He and N. Q. Zhao, *J. Mater. Chem.*, 2012, **22**, 1297–1304.
22 N. T. K. Thanh, N. Maclean and S. Mahiddine, *Chem. Mater.*, 2014, **26**, 5–21.
23 Y. Hong, H. J. Kim, D. Yang, G. Lee, K. M. Nam, M. H. Jung, Y. M. Kim, S. Choi and W. S. Seo, *Nano Res.*, 2017, **10**, 2866–2880.